13th World Conference on Earthquake Engineering
Vancouver, B.C., Canada
August 1-6, 2004
Paper No. 3256

TOUCHING ANALYSIS OF TWO BUILDINGS USING FINITE ELEMENT METHOD

Mircea IEREMIA[1], Silviu GINJU[1], Adrian Ivan[2]

SUMMARY

The present paper focuses on the contact-impact analysis of two buildings during the 1977 Vrancea Earthquake, Romania.

The strength structure, for both of them, is made up of steel frame. The buildings have different heights, lateral stiffness and masses. A Time history analysis in elasto-plastic range of steel behaviour has been accomplished, in order to model the impact. Thus, for modeling the contact of these two buildings Gap finite elements are being used. So, this analysis shows the individual vibration characteristics of each building but also, the deformations and forces resulted from the contact in the structures.

This paper points out both the necessity of a certain determination for computing the gap between two new buildings, as well as the method of analysis for the old buildings with unsuitable gaps between them.

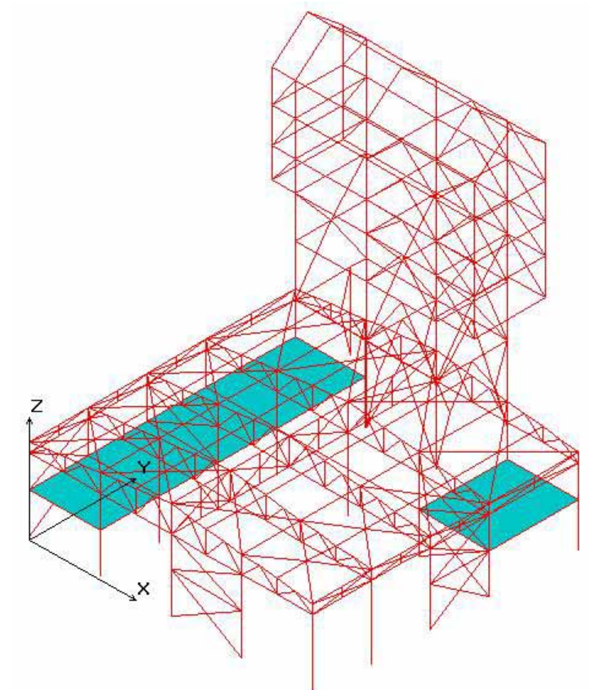

Figure 1. The discretization in finite elements of two buildings structure

[1] Prof. dr., Technical University of Civil Engineering Bucharest, Romania. Email:mieremia@mail.utcb.ro
[2] Prof. dr., Politechnical University of Timisoara, Romania. Email: aivan@ceft.utt.ro

INTRODUCTION

The paper presents the modal and nonlinear dynamic analysis of two buildings in earthquake interaction (figure 1).

The higher building (figure 2) is a station for coal distribution, nitrogen and oxygen strength structure, afferent to F2 furnace, belonging to S.C. SIDEX S.A. Galati, Romania. The Distribution Station has 4 technological levels.

The strength structure is made up of many-stored bracing steel frames, being assembled by welding. The building has 4 levels of 6m height, one span of 6m and two bays of 6m. In the gable, the building has two consoles about 3.20m and 1.95m respectively. The Station is parallel with the furnace house. The building is covered with iron pleated.

The building is supported by foundation plates up to the –2.20m depth and by drilling piles of 800 mm diameter beyond that.

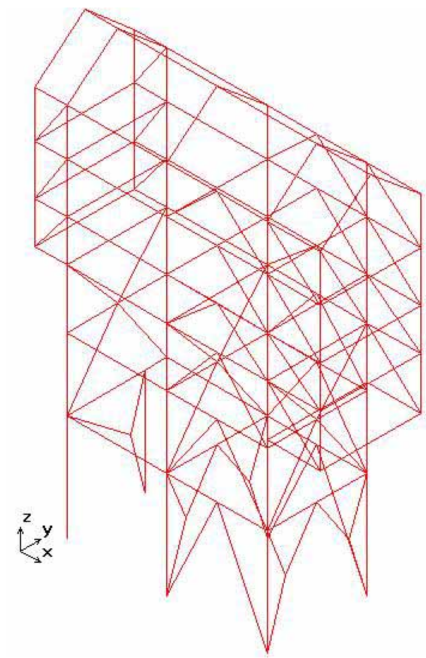

Figure 2. The high structure

The access in the Station is done through a gangway being supported by the furnace house and the stairs between the floors. Between the furnace house and the Station there are some pipes which penetrate in the Station from where the connections with the furnace are made.

The lower building (figure 3) is an industrial hall with ground floor and partial first floor. The ground floor space is used as storage space and the first floor houses offices. The strength structure is made of metallic farms with stiffness bars vertically as well as horizontally. The pillars transmit the loads to the foundation land through some isolated foundations.

Between the two buildings there is an earthquake distance of 3 cm.

The buildings have the ‚C' category of importance in accordance with H.G. 766/1997, and III in accordance with P100-92 standard. The buildings are placed in ‚C' seismic zone with Tc=1.5 period of corner and Ks=0.20, seismic zone coefficient.

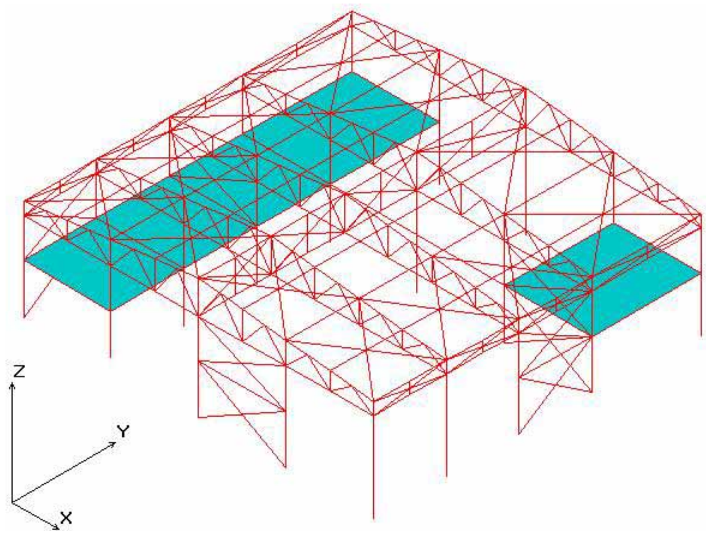

Figure 3. The lower structure

CONSIDERATIONS REGARDING THE MODELLING

The strength of both structures has been analysed using a finite element method. For this purpose the high structure has been divided into 214 BEAM finite elements connected in 90 nodes. For defining the sections of the elements three constants' sets have been necessary. The columns have I cross-section composed of welding steel (flange: 350x20, web: 500x15), the bracings are made up of two U20 laminated channel section and the beams have I cross-section composed of welding steel (flange: 240x15, web: 400x8).

The lower structure has been divided into 554 BEAM finite elements connected in 232 nodes. The columns has wide flange cross-section composed of welding steel (flange: 180x20, web: 450x12), the vertical bracings are made up of pipe ∅140/8 section, the horizontal bracings are made up of angle 100x100x10 section, the purling are made up of two U20 laminated channel section and the frame girders have flange composed of two 140x140x40 angle section and the truss of frame girder is composed of two 140x140x40 angle section.

All the steel elements are made of OL37. For the simulation of the steel elements in elasto-plastic range, BEAM finite element with von Mises constitutive law has been used. The interaction between the structures was modelled with Gap finite elements.

CONSIDERATIONS REGARDING THE DYNAMIC ANALYSIS

Linear modal analysis

The moving equation for an undamped dynamic system, expressed in matrix notation is:

$$[M]\{\ddot{u}\} + [K]\{u\} = \{0\} \tag{1}$$

where:

[M] – the structure mass matrix;

[K] – the structure stiffness matrix in elastic range.

For a linear system, free vibrations will be harmonic having the form:

$$\{u\} = \{\phi\}_i \cos \omega_i t \tag{2}$$

where: $\{\phi\}_i$ - eigenvector representing the mode shape of the i-th natural frequency;

ω_i - i-th natural circular frequency (radians per unit time);

t - time.

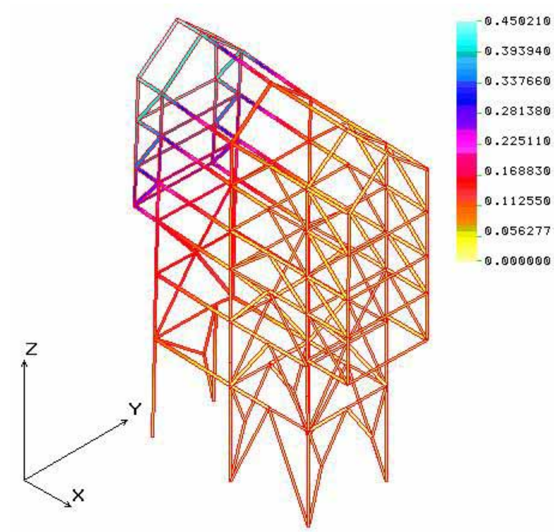

Figure 4. High structure. The first mode of vibration

Thus, equation (1) becomes:

$$(-\omega^2 [M] +[K]) \{\phi\}_i = \{0\} \quad (3)$$

This equation is satisfied if either $\{\phi\}_i$ is zero or the determinant of $(-\omega^2[M]+[K])$ is zero. The first option is the trivial one and, therefore, is not of interest. Thus, the second one gives the solution:

$$\left| [K] -\omega^2 [M] \right| = 0 \quad (4)$$

This is the standard form of eigenvalues equation which must be solved for up to n values of ω^2 and n eigenvectors $\{\phi\}_i$ which satisfy equation (3), where n is the number of DOF's.

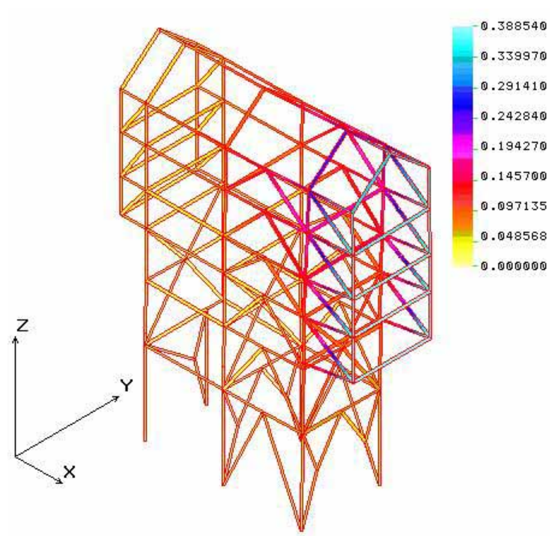

Figure 5. High structure. The 2-th mode of vibration

The eigenvalue and eigenvector problem needs to be solved for mode-frequency analysis. It has the form of:

$$[K]\{\phi_i\} = \lambda_i [M]\{\phi_i\} \qquad (5)$$

where:

λ_i - the eigenvalue.

By applying this type of analysis, the eigenvalues and eigenvectors of the first 20 modes of vibratoins have been obtained. The rate of modal mass participation obtained for horizontal vibrations is ~90%, and for vertical vibrations is ~80%.

Due to the obtained first period of T_1 = 0.87 s, the structure is considered a semi-flexible structure.

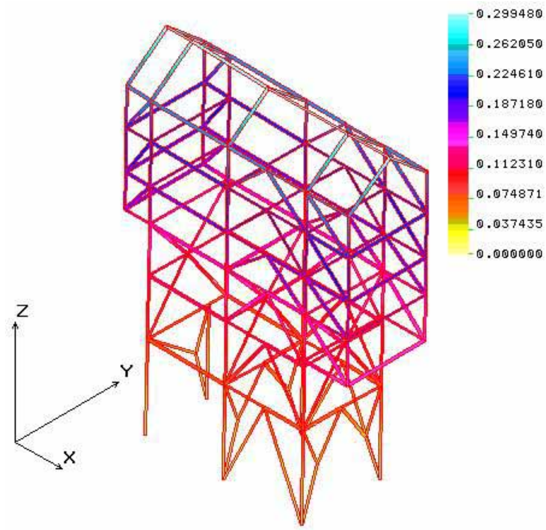

Figure 6. High structure. The 3-th mode of vibration

Table1. High structure. Eigenvalue and mass participation factors

Mode	ω (rad/s)	ν (hertz)	T (s)	Fpx (%)	Fpy (%)
1	7.21	1.14	0.87	0.07	35.70
2	8.47	1.34	0.74	0	42.20
3	14.80	2.35	0.42	93.70	0
4	16.38	2.60	0.38	1.09	6.67
5	17.80	2.83	0.35	0.02	0.39
6	19.22	3.05	0.32	0	2.55
7	20.87	3.32	0.30	0.02	0.78
8	29.40	4.67	0.21	0	3.23
9	30.18	4.80	0.20	0	0.42
10	32.87	5.23	0.19	0	0.88

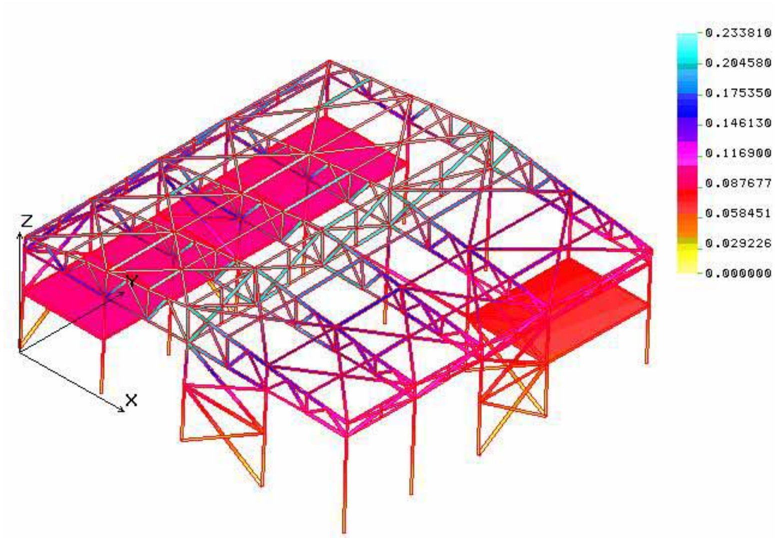

Figure 7. Lower structure. First mode of vibration

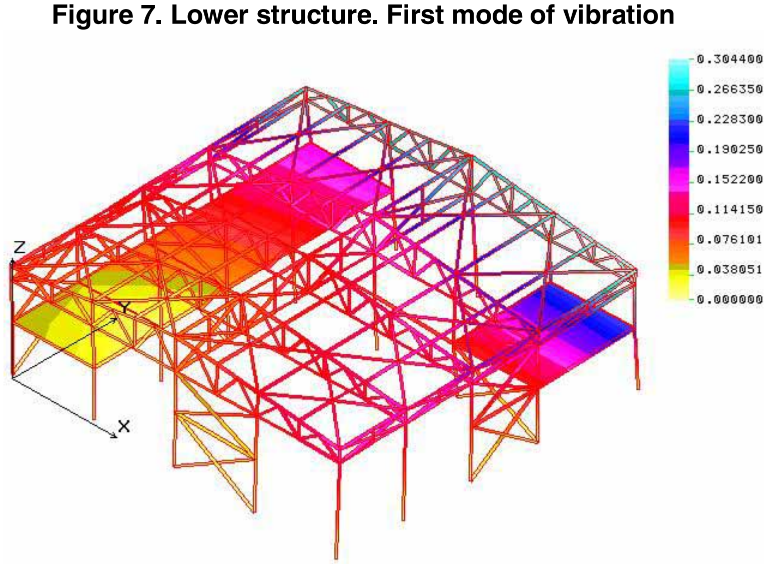

Figure 8. Lower structure. The 2-th mode of vibration

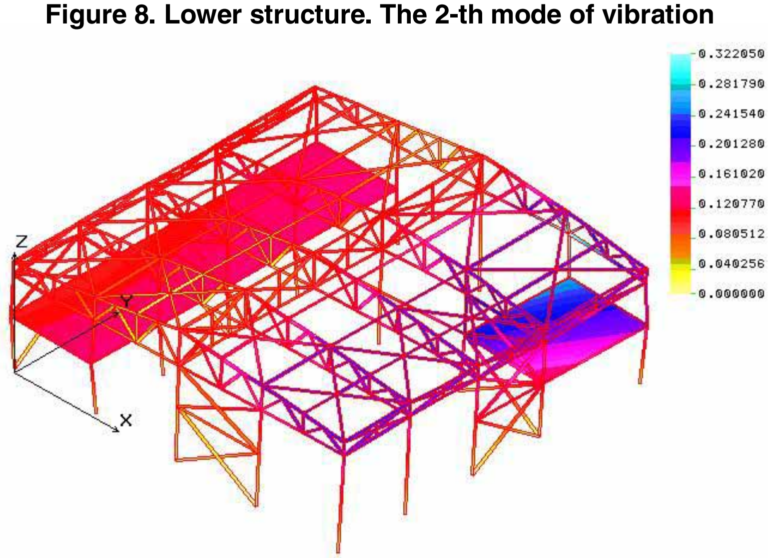

Figure 9. Lower structure. The 3-th mode of vibration

Table 2. Lower structure. Eigenvalue and mass participation factors

Mode	ω (rad/s)	ν (hertz)	T (s)	Fpx (%)	Fpy (%)
1	19.17	3.05	0.32	0.26	83.5
2	26.34	4.19	0.23	47.7	0.45
3	28.84	4.59	0.21	5.31	0.23
4	33.88	5.39	0.18	32.7	0.83
5	34.10	5.42	0.17	4.91	3.96
6	39.87	6.34	0.15	0.04	6.90
7	54.54	8.68	0.11	0	26.1
8	63.76	10.14	0.09	0.86	0.54
9	68.82	10.95	0.09	3.89	0
10	72.55	11.54	0.08	1.10	0.65

Time history analysis

The strength structures have been dynamically analyzed using the directly integration method of the differential motion equation, considering the damping influence in structure's dynamic response.

When using the finite element method for structures' discretization, the moving equations system becomes:

$$[\mathrm{M}]\{\ddot{U}(t)\}+[C]\{\dot{U}(t)\}+[K]\{U(t)\}=-[M]\{\ddot{u}(t)\} \tag{8}$$

Using the Newmark [1] integration scheme, we can make the following assumptions:

$$\dot{U}_{t+\Delta t}=\dot{U}_t+\left[(1-\delta)\ddot{U}_t+\delta*\ddot{U}_{t+\Delta t}\right]\Delta t \tag{9}$$

$$U_{t+\Delta t}=U_t+\dot{U}_t\Delta t+\left[\left(\frac{1}{2}-\alpha\right)\ddot{U}_t+\alpha*\ddot{U}_{t+\Delta t}\right]\Delta t^2, \tag{10}$$

where: α si β are the parameters which give the stability and accuracy of the integration process.

For solving the displacements, speeds and accelerations at t+Δt time, we considered the equations (9), (10) and also the equilibration equations at t+Δt time:

$$M\ddot{U}_{t+\Delta t}+C\dot{U}_{t+\Delta t}+KU_{t+\Delta t}=R_{t+\Delta t} \tag{11}$$

Solving the equation (10) for $\ddot{U}_{t+\Delta t}$ varying with $U_{t+\Delta t}$ and then placing the obtained relation in (9), we obtain the equations for $\ddot{U}_{t+\Delta t}$ si $\dot{U}_{t+\Delta t}$. Both of them varying only with the unknown displacements $U_{t+\Delta t}$. These two equations for $\dot{U}_{t+\Delta t}$ si $\ddot{U}_{t+\Delta t}$ are placed in (11) to find out $U_{t+\Delta t}$. Then, using the equations (9) and (10) it obtains acceleration $\ddot{U}_{t+\Delta t}$ and speeds $\dot{U}_{t+\Delta t}$.

The complete algorithm using the Newmark integration scheme is made of:

_*The first computations:*

- it forms the matrix K (of stiffness), M (of masses) and C (of damping);
- it gives to the displacement, speed and respectively acceleration, one first value: $U_0, \dot{U}_0 si \ddot{U}_0$
- it selects Δt – step of time, α and δ parameters, and also, the integration constants are computed:

$$a_0=\frac{1}{\alpha\Delta t^2};\quad a_1=\frac{\delta}{\alpha\Delta t};\quad a_2=\frac{1}{\alpha\Delta t^2};\quad a_3=\frac{1}{2\alpha};\quad a_4=\frac{\delta}{\alpha}-1;$$

$$a_5=\frac{\Delta t}{2}\left(\frac{\delta}{\alpha}-2\right);\quad a_6=\Delta t(1-\delta);\quad a_7=\delta\Delta t;$$

$$\delta \geq 0.50; \ \alpha \geq 0.25\ (0.50+\delta)^2 \quad (12)$$

- it forms the stiffness matrix:

$$\hat{K} : \hat{K} = K + a_0 M + a_1 C \quad (13)$$

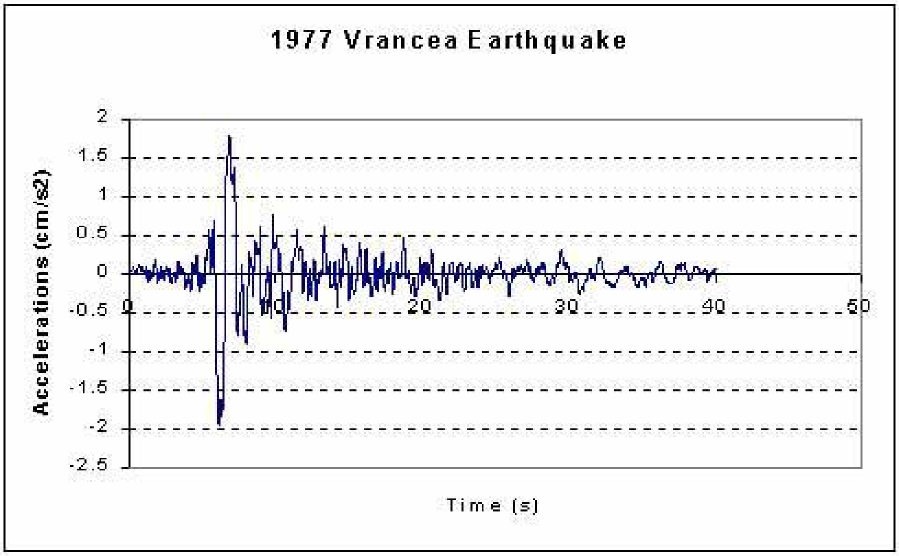

Figure 10. The 1977 Vrancea earthquake

For each time-step:

- it calculates loading for t+Δt step of time:

$$\hat{R}_{t+\Delta t} = R_{t+\Delta t} + M\left(a_0 U_t + a_2 \dot{U}_t + a_3 \ddot{U}_t\right) + C\left(a_1 U_t + a_4 \dot{U}_t + a_5 \ddot{U}_t\right) \quad (14)$$

- it calculates the displacement for t+Δt step of time:

$$\hat{K}\ U_{t+\Delta t} = \hat{R}_{t+\Delta t} \quad (15)$$

- it calculates the accelerations and speeds for the t+Δt step of time:

$$\ddot{U}_{t+\Delta t} = a_0\left(U_{t+\Delta t} - U_t\right) - a_2 \dot{U}_t - a_3 \ddot{U}_t$$

$$\dot{U}_{t+\Delta t} = \dot{U}_t + a_6 \ddot{U}_t + a_7 \ddot{U}_{t+\Delta t}$$

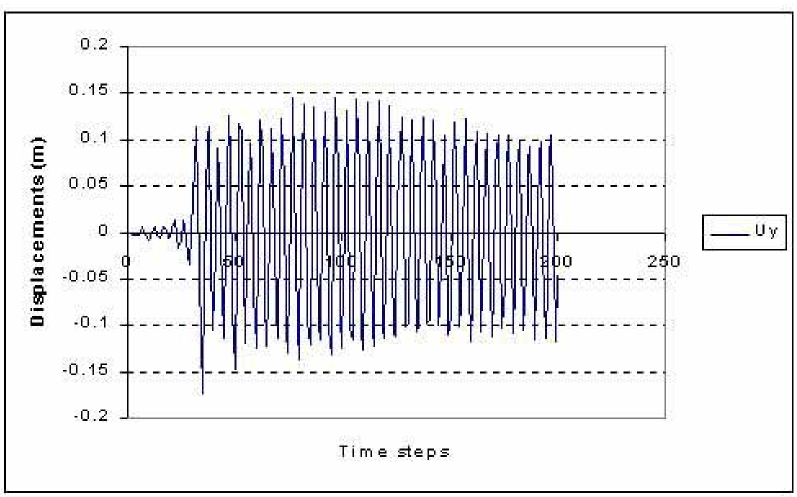

Figure 11. High structure response

For simulating the dynamic action of the earthquake, the 1977 Vrancea recordings (Figure 10) have been used. The earthquake has a magnitude of M=7.4 and the following characteristics:

- ground accelerations 0.20g;
- the maximum displacement at the ground level 3.7 cm;
- the length of action 42 sec.

The recorded acceleration graph have been divided in 200 steps having the first case of loading: dead loadings (the weight of the structure) and live loadings placed on the floors.

The response of high structure in elasto-plastic range is presented in figure 11. The low structure, during the earthquake action, is in elastic range (figure 12).

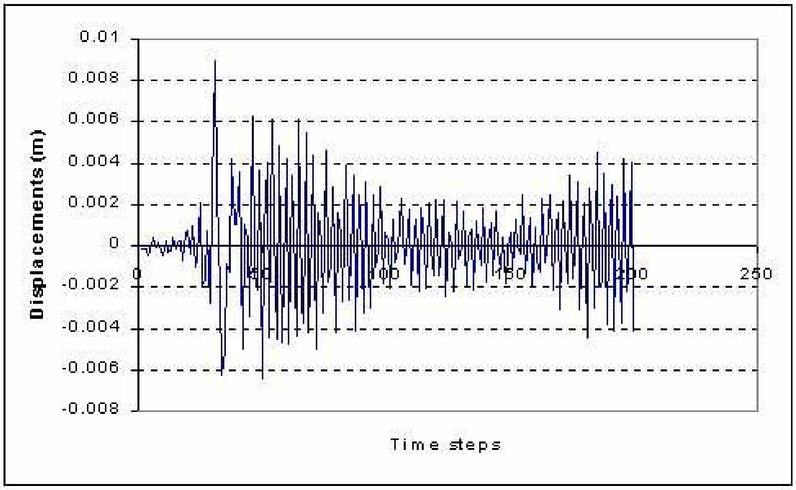

Figure 12. Lower structure response

THE CONSTITUTIVE RULE OF THE MATERIAL

The constitutive Von Misses [2] rule of the steel with cinematic consolidation has been used in time-history analysis for modelling the behaviour in elasto-plastic range.

The expression of the equivalent stress is :

$$\sigma_e = [\frac{3}{2}(\{s\} - \{a\})^T [M](\{s\} - \{a\})]^{1/2} \tag{17}$$

where:

$\{s\}$ – the deviatoric stress vector;

$$\{s\} - \{\sigma\} - \sigma_m [\,1 \quad 1 \quad 1 \quad 0 \quad 0 \quad 0\,]^T \tag{18}$$

where:

$$\sigma_m = \frac{1}{3}(\sigma_x + \sigma_y + \sigma_z) \tag{19}$$

σ_m – the mean of hydrostatic stress;

$\{a\}$ – the yield surface translation vector.

Note that since the equation (17) is dependent on the deviatoric stress, yielding is independent of the hydrostatic stress. When equivalent stress σ_e is equal to the uniaxial yield stress, σ_y , the material is assumed to yield.

The yield criterion is therefore:

$$F = [\frac{3}{2}(\{s\} - \{a\})^T [M](\{s\} - \{a\})]^{1/2} - \sigma_y = 0 \quad (20)$$

The associated flow rule yields:

$$\left\{\frac{\partial Q}{\partial \sigma}\right\} = \left\{\frac{\partial F}{\partial \sigma}\right\} = \frac{3}{2\sigma_e}(\{s\} - \{a\}), \quad (21)$$

so, the increment in plastic strain is normal to the yield surface. The associated flow rule with the von Mises yield criterion is known as the Prandtl – Reuss flow equation.

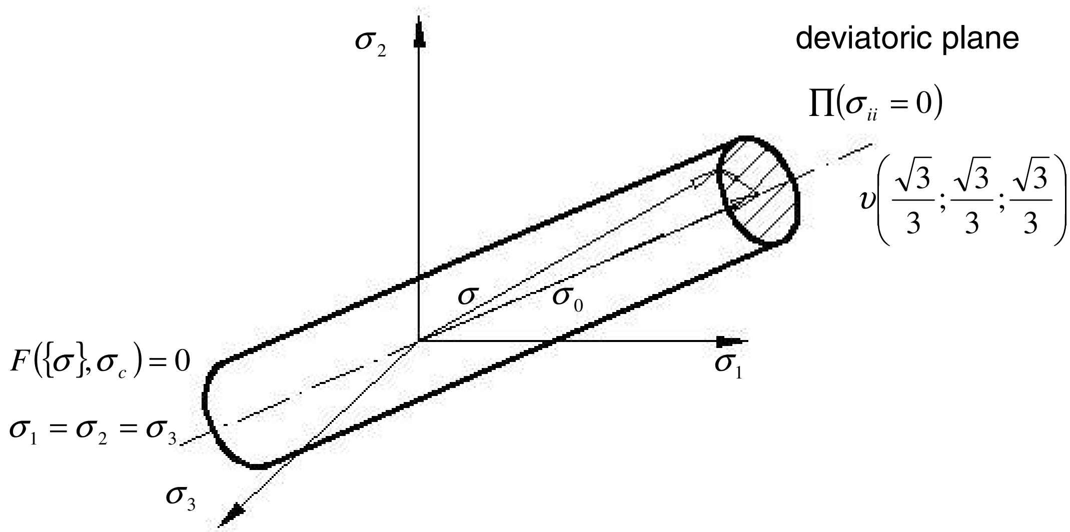

Figure 13. The von Mises yield criterion

The yield surface translation is defined as:

$$\{a\} = 2G\,\{\varepsilon^{sh}\} \quad (22)$$

where:

G – the transversal shear modulus;

The increment deformation is analogously computed with (23) equation:

$$\{\varepsilon_n^{sh}\} = \{\varepsilon_{n-1}^{sh}\} + \{\Delta\varepsilon^{sh}\} \quad (23)$$

where:

$$\{\Delta\varepsilon^{sh}\} = \frac{C}{2G}\{\Delta\varepsilon^{sh}\} \quad (24)$$

and:

$$C = \frac{2}{3}\frac{EE_T}{E - E_T} \quad (25)$$

where:

E – the longitudinal Young's modulus;

E_T – the tangent modulus from the bilinear uni-axial stress-strain curve.

The yield surface translation $\{\varepsilon^{sh}\}$ is initially zero and changes with subsequent plastic straining.

The equivalent plastic strain is dependent on the loading history and is defined :

$$\hat{\varepsilon}_n^{pl} = \hat{\varepsilon}_{n-1}^{pl} + \Delta\hat{\varepsilon}^{pl} \qquad (26)$$

where:

$\hat{\varepsilon}_n^{pl}$ - the equivalent plastic strain for this time point;

$\hat{\varepsilon}_{n-1}^{pl}$ - the equivalent plastic strain from the previous time point.

The equivalent stress parameter is defined :

$$\hat{\sigma}_e^{pl} = \sigma_y + \frac{EE_T}{E - E_T}\hat{\varepsilon}_n^{pl} \qquad (27)$$

where:

$\hat{\sigma}_e^{pl}$ - the equivalent stress parameter.

Note that when there is no plastic strain ($\hat{\varepsilon}^{pl} = 0$), $\hat{\sigma}_e^{pl}$ is equal to the σ_y yield stress.

If the load were to be reversed after plastic loading, the stress σ_e would fall bellow yield, but $\hat{\sigma}_e^{pl}$ would register above (since $\hat{\varepsilon}^{pl}$ is non zero).

CONSIDERATIONS REGARDING THE TIME HISTORY ANALYSIS

The seismic interaction of the two structures has been dynamically analysed in four types of placement. Thus, the following distances between buildings have been considered: 0 cm, 1 cm, 2 cm, 3 cm, the last choice representing the genuine placement of the buildings. Following the performance of the 4 time history analysis, the seismic forces dissipated through collision have been rendered in graphs (figures 14÷17). For the earthquake distance of 0 cm (figure 14), the interaction between the two structures is unfolded through out the duration of the seism. The second situation analysed, that of the earthquake distance of 1cm (figure 15), shows that the structures interact between the moment of PGA (peak ground acceleration) and the end of the acceleration graph. For an earthquake distance of 2 cm (figure 16), 8 collisions between the buildings are noticed. A single collision occurs for the earthquake distance of 3 cm (figure 17).

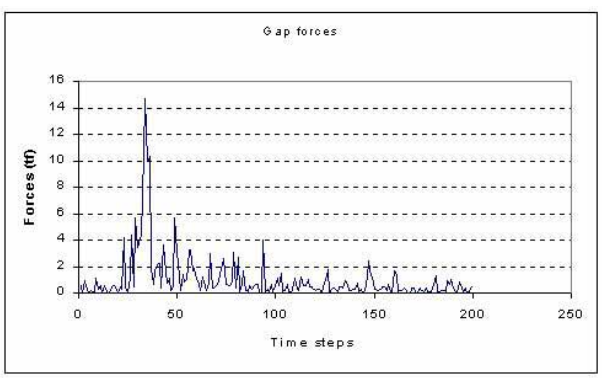

Figure 14. Gap forces for 0 cm

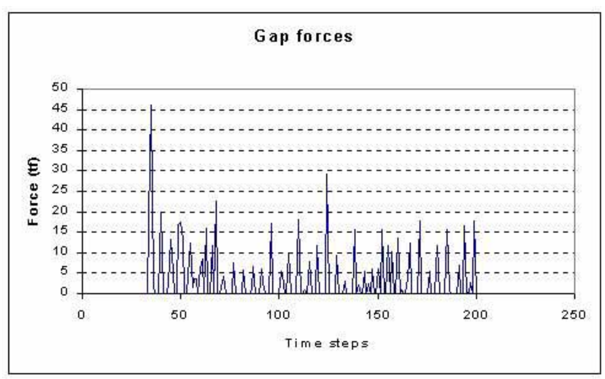

Figure 15. Gap forces for 1 cm

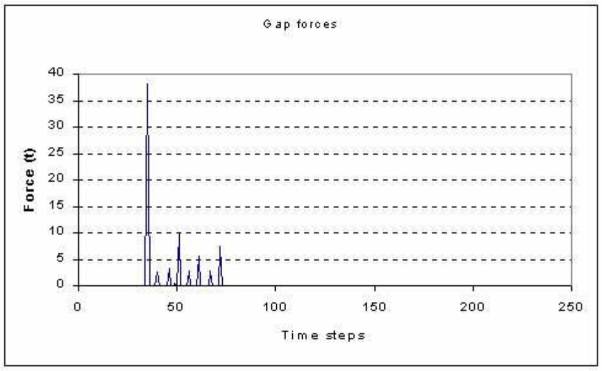

Figure 16. Gap forces for 2 cm

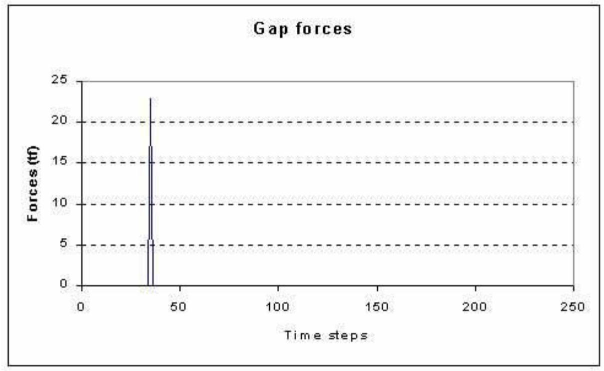

Figure 17. Gap forces for 3 cm

The movement response of structures in the four cases of interaction is rendered by comparison with the case when the structures do not interact.

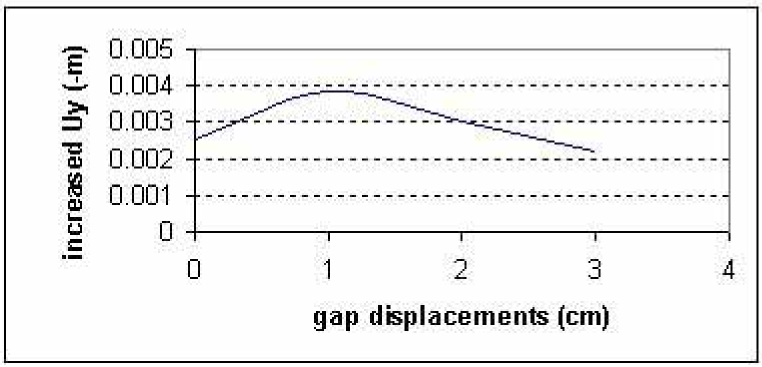

Figure 18. Lower structure. Negative increased displacements

Figure 18 shows the variation of negative maxims to the low structure response for the 4 cases of earthquake distance. The variation of positive maxims of the low structure response for the 4 cases of earthquake distance is rendered in figure 19. Similarly, in figure 20 are presented the negative maxims' variation whereas in figure 21 the positive maxims variation in displacements for the high structure response, regarding the 4 types of earthquake distance.

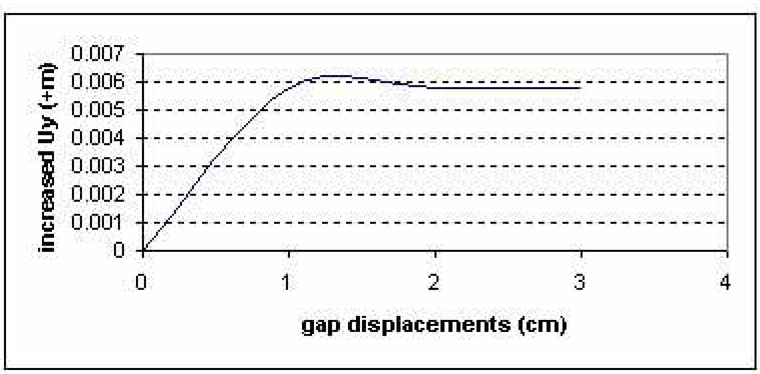

Figure 19. Low structure. Positive increased displacements

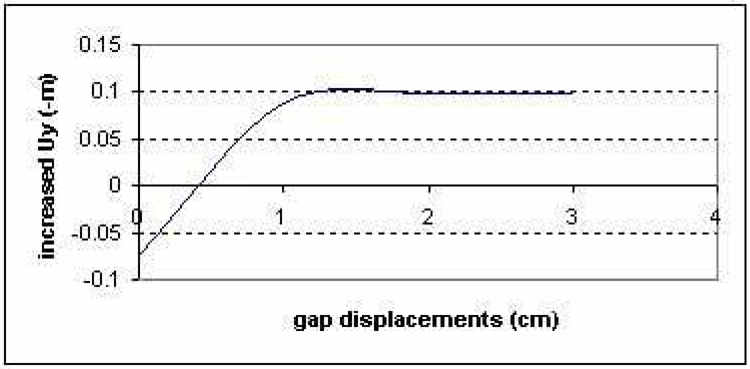

Figure 20. High structure. Negative increased displacements

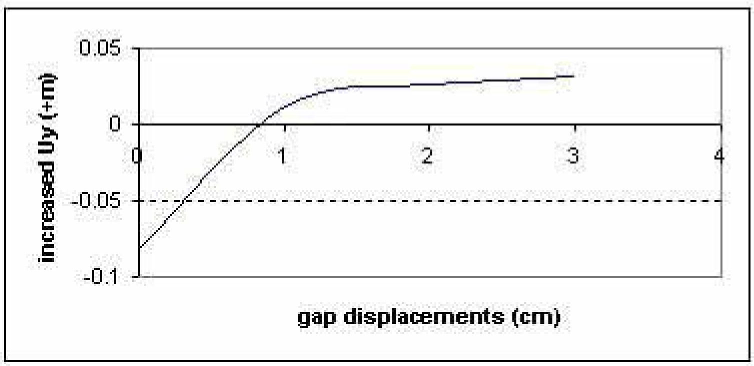

Figure 21 High structure. Pozitive increased displacements

CONCLUSIONS

The independent analysis of the two strength structures having different masses and rigidities, showed different response to seismic action. Thus, as a result of the seismic action, the low structure remains in the elastic field of behaviour for steel, while the high structure displays a mainly elasto-plastic behaviour. The two buildings are differently influenced by the size of the earthquake distance. Thus, the low building is influenced more by the 1cm earthquake distance, while a 3cm earthquake distance has major influences on the high building. Also, as a result of collision, the lower structure suffers minor local plastifications, while for the higher building the dynamic amplification involves major elasto-plastic changes, and also in elements located outside the contact area.

For the case when there is no gap between the buildings, no major amplification of dynamic response upon seismic action occurs for none of the buildings, the dissipation of seismic energy through moderate collisions occurring through out the duration of the seismic movement.

This fact might partially explain why buildings which do not comply with seism safety standards have not collapsed during major earthquakes.

REFERENCECS

[1] K.J.Bathe, "Finite Element Procedures", Prentice Hall, Englewood Cliffs, New Jersey, U.S.A, 1996.
[2] M.Ieremia, "Elasticity.Plasticity.Nonlinearity.", Ed.PRINTECH Bucharest, Romania, 1998.